Available online at www.sciencedirect.com
ScienceDirect
Acta Materialia 54 (2006) 5209–5220
Acta MATERIALIA
www.actamat-journals.com

# Non-isothermal tensile tests during solidification of Al–Mg–Si–Cu alloys: Mechanical properties in relation to the phenomenon of hot tearing

D. Fabrègue [a,*], A. Deschamps [a], M. Suery [b], J.M. Drezet [c]

[a] LTPCM, UMR CNRS 5614, Institut National Polytechnique de Grenoble, Domaine Universitaire, BP75, 38402 St Martin d'Hères, France
[b] GPM2, UMR CNRS 5010, ENSPG-BP46, 101 Rue de la Physique, Domaine Universitaire, BP46, 38402 Saint Martin d'Hères, France
[c] LSMX, EPF-Lausanne, MX-G Ecublens, Station 12, CH-1015, Lausanne, Switzerland

Received 11 April 2006; received in revised form 19 June 2006; accepted 19 June 2006
Available online 25 September 2006

**Abstract**

An original set-up has been used to study the mechanical properties of aluminium alloys in tension during solidification with a high cooling rate (70 K $s^{-1}$). The mechanical behaviour of 6056 aluminium alloy with and without grain refiner has been investigated as well as that of mixtures between AA6056 and AA4047. The results show that the alloys exhibit a viscoplastic behaviour in the mushy state. A transition is observed between fracture in the mushy state and fracture in the solid state as a function of the displacement rate. This displacement rate at the transition depends on the cooling rate and on the composition of the alloy. The displacement before fracture is observed to be independent of displacement rate but to depend on the composition and on the solidification rate. Based on the observations a criterion for fracture in the mushy state is proposed. A simple rheological law describing the mechanical behaviour of the alloys is coupled to a finite element calculation giving the thermal field during the tensile test. This simulation is able to reproduce the mechanical response of the solidifying alloy during a non-isothermal test.


*Keywords:* Tension test; Semi-solid processing; Aluminium alloys; Hot tearing laser welding

## 1. Introduction

The mechanical response of partially solidified metallic alloys subjected to straining is an investigation field of wide interest [1–5]. From the practical viewpoint, this response needs to be understood to control material processing where substantial deformation occurs in the mushy state, either on purpose as in thixo-forming [6], or inevitably as in the casting of ingots [7–10], or during welding [11,12]. In the latter processes, thermal contraction, shrinkage associated with solidification, and the boundary conditions of the process exert tensile stresses on the material in the mushy state. It is well known that these tensile stresses, when acting at low liquid fractions, can lead to macroscopic failure (hot tearing) [13–15]. It is therefore crucial to understand quantitatively the mechanical behaviour of these materials, both in terms of stress–strain response and in terms of fracture mechanisms.

Characterising the mechanical behaviour in the mushy state is not an easy task. As far as the conditions where hot tearing occurs are concerned, the interesting fractions of solid comprise between 0.9 and 1 [16,17]. The temperature interval corresponding to this range of solid fractions may be very small, depending on the alloy system. Moreover, it has been repeatedly shown in the literature that the mechanical properties in the mushy state are highly dependent on the thermal path: in fact, the mechanical

* Corresponding author. Present address: Université Catholique de Louvain, UCL-IMAP, Place Sainte Barbe 2, B-1348 Louvain-la-Neuve, Belgium. Tel.: +32 10 47 35 65.
*E-mail address:* fabregue@imap.ucl.ac.be (D. Fabrègue).

1359-6454/$30.00 
doi:10.1016/j.actamat.2006.06.027

properties obtained at identical fractions of solid are very different if the material is solidified in situ before the mechanical test, or if it is re-melted from a fully solid sample [18,19]. In addition, in many practical cases, such as during the solidification of a weld pool, deformation of the solidifying material occurs non-isothermally. The mechanical behaviour in such non-isothermal conditions has not received much attention until now [20].

This paper presents a detailed study of the mechanical behaviour of several aluminium alloys, based on AA6056 + AA4047 mixtures, during non-isothermal straining in the mushy state. Mixing these two alloys is representative of the composition of the nugget of laser welds of AA6056 plates with AA4047 filler wire. Indeed, increasing the Si content in the weld pool is known to decrease sensitivity to hot tearing [8,15]. Constant crosshead velocity tests were carried out at relatively high cooling rates (25 and 70 K $s^{-1}$), the material being solidified in situ in the tensile machine before straining started at a given solid fraction. The studied parameters include the cooling rate, the strain rate, and the chemical composition of the alloy. The variation of stress during these experiments is discussed, and modelled using a constitutive law based on isothermal experiments, published in a previous paper [3]. The dependence of fracture mode on the different testing parameters is investigated, and a failure criterion is proposed.

## 2. Experimental

### 2.1. Synthesis of the alloys

The AA6056 alloy was supplied by ALCAN as plates, 6 mm in thickness. It was received in the T4 condition (solution heat treated followed by natural ageing). The composition of this alloy (all concentrations in the following are in wt.%) and of the filler wire (AA4047) are given in Table 1. The filler wire was 1 mm in diameter. Different alloys were investigated: the original 6056 alloy and two alloys obtained by mixing 6056 and 4047, with a resulting Si concentration of, respectively, 2 wt.% (typical of laser weld nuggets) and 4 wt.%. These alloys were used to study the influence of the Si concentration on the mechanical behaviour. A fourth alloy was obtained by adding a grain refiner to the original 6056 in order to quantify the influence of the grain size. In this case, 5 g/kg of ATi5B (Al–5%Ti–1%B), which is a typical industrial grain refiner, was used. In all cases, the materials were melted in a furnace using a graphite crucible coated with boron nitride, and subsequently cast in a boron nitride-coated stainless steel mould and air-cooled. The pouring temperature was 720 °C and since the steel mould was not preheated, the average cooling rate in the mushy zone was about 1 K $s^{-1}$. Fig. 1 shows the initial microstructure of the cast samples.

Table 1
Composition (wt.%) of the 6056 and 4047 alloys

| Alloy | Mg | Si | Cu | Mn | Fe |
|---|---|---|---|---|---|
| 6056 | 0.86 | 0.92 | 0.87 | 0.55 | 0.19 |
| 4047 | 0.1 | 12 | 0.3 | 0.15 | 0.8 |

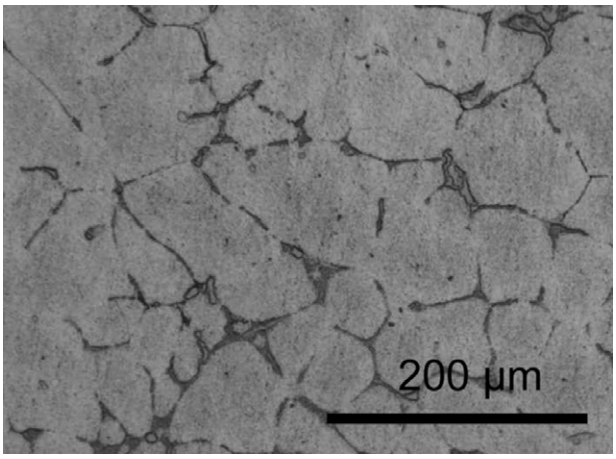


Fig. 1. Microstructure of the as-cast 2% Si alloy.

### 2.2. Experimental set-up for non-isothermal tensile testing

In order to perform non-isothermal tensile tests with a high cooling rate, a specific experimental set-up was designed. The tests were carried out using an ADAMEL DY 34 tensile machine with a 2 kN load cell. The sample was heated by induction using an inductive copper coil with a power of 5 kW. The samples were machined from the ingots obtained as explained in Section 2.1. The sample geometry is shown in Fig. 2. The two M5 holes allowed screwing water flow pipes to ensure a high cooling rate of the sample during the whole test. A type K thermocouple with a diameter of 0.5 mm was introduced in a hole drilled at 14° off the specimen axis (Fig. 2) in order to measure the temperature at the very centre of the sample. The thermocouple was coated with boron nitride to protect it from liquid aluminium. Measurements were carried out to check that the boron nitride coating did not affect the temperature measurement. As the centre of the sample was fully melted during the test, a crucible was placed around the central part of the sample to hold the liquid bath. Two types of crucible were used, made of alumina and graphite. In the first case, the crucible itself was not heated by induction during the heating stage of the aluminium sample; therefore during the cooling stage the cooling rate was a maximum, at approximately 70 K $s^{-1}$. In the second case, the crucible was the main heat source during the heating stage, thus more heat had to extracted during the cooling stage, resulting in a reduced cooling rate of about 25 K $s^{-1}$.

### 2.3. Test procedure

Since the tensile tests were carried out in a non-conventional manner, it is important to detail the test procedure

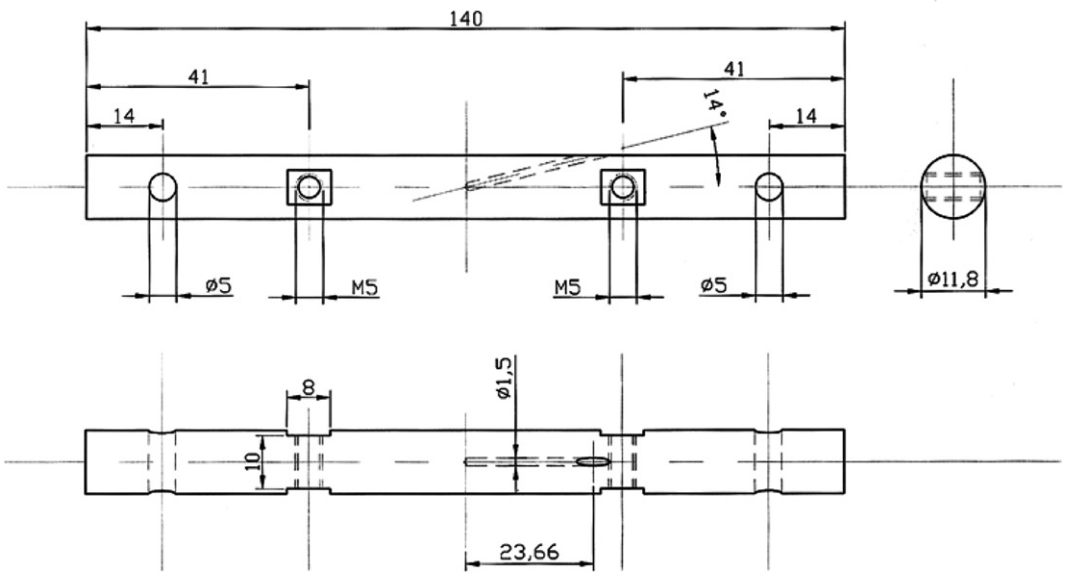


Fig. 2. Sample geometry for the non-isothermal tensile tests.

which was systematically used for all the experiments. Firstly, the specimen was attached to the fixed grip of the tensile testing machine. Then it was cooled by the water pipes until it reached the temperature of the cooling water. It was then attached to the moving grip of the machine and heated by the inductive coil. During heating of the middle part, the water was still flowing through the sample. Dilatations due to thermal expansion of the sample were automatically accommodated by regulating the load to zero. When the temperature in the central part of the specimen reached about 700 °C, which means that this part is fully liquid, the temperature was held for 15 s (Fig. 3). The inductive coil was then shut off and the temperature began to decrease. When the desired temperature for the beginning of the tensile test was attained, the predefined program started the tensile machine at a given displacement rate and the load was recorded during the test. All the tests presented here were carried out using a solid fraction of 0.84 as a starting point of the loading. This fraction was chosen to observe the behaviour in the mushy state. Lower starting solid fractions involve rapid fracture (absence of ductility) whereas higher solid fractions lead to fracture in the solid state.

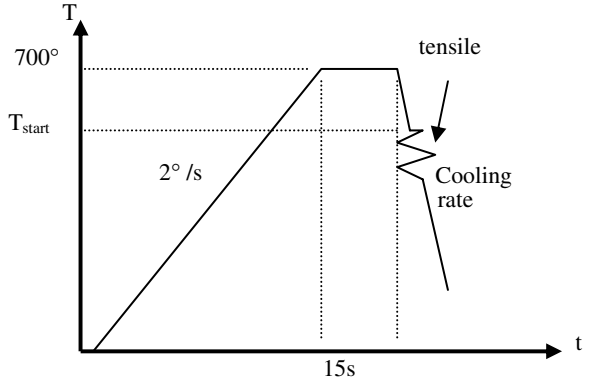


Fig. 3. Thermal cycle representative of the non-isothermal tensile test.

### 2.4. Fractions of solid as a function of temperature

The evolution of the fraction of solid with temperature for the three alloys under study was evaluated using the ALCAN software Prophase [21]. This software assumes infinite diffusion in the liquid phase and takes into account a limited back diffusion of the alloying elements in the solid phase. The calculations of the solid fraction were performed for a cooling rate of 10 K $s^{-1}$ (which represents the maximum solidification speed taken into account by the software) representative of the experimental cooling rate. The difference between this cooling rate and that used in the calculations is believed to have a negligible influence on the solid fraction at a given temperature, since for both cooling rates back diffusion in the solid is very limited.

### 2.5. Compression tests at high temperature

In addition to experiments carried out during solidification, experiments were performed to characterise the behaviour of the alloys in the solid state. For these experiments, compression test cylinders with a diameter of 12 mm and a height of 18 mm were machined. Before testing, the samples were homogenised for 24 h at 480 °C. The compression tests were carried out using an ADAMEL DY35 machine equipped with a radiant tube furnace. The heating rate was 20 K $min^{-1}$ and the compression tests were strain rate controlled using the mechanical cycle given in Fig. 4. The force was measured using a 20 kN load cell and the strain was calculated using the crosshead displacement. The compression tests were conducted at

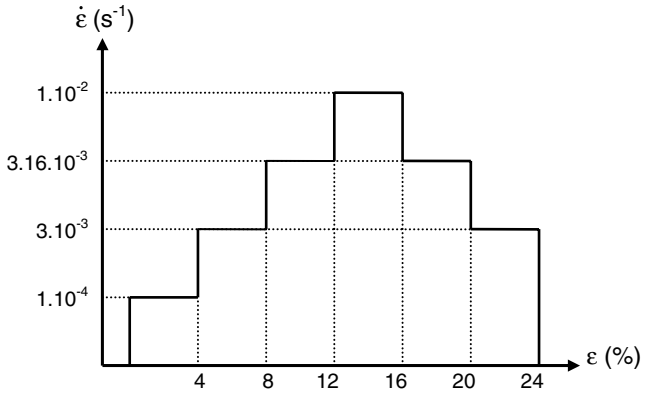


Fig. 4. Mechanical cycle applied to compression samples in the solid state: strain rate imposed as a function of the measured strain.

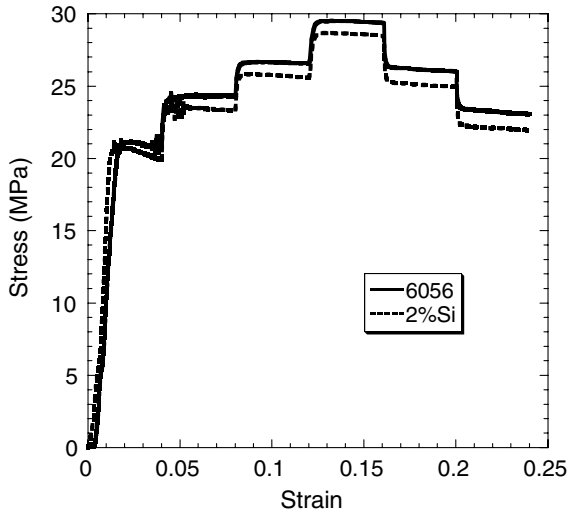


Fig. 5. Measured stress as a function of strain during compression tests at 450 °C carried out with the two alloys.

four different temperatures (450, 475, 510, and 530 °C) which were measured using a type K thermocouple inserted in the lower grip right under the surface. As an example, Fig. 5 presents the results of a compression test at a temperature of 450 °C for the 6056 alloy and the alloy containing 2 wt.% Si.

## 3. Results

### 3.1. Microstructure and fracture surfaces

The experimental set-up used in this study was aimed at gaining a better understanding of the occurrence of hot tearing during solidification processes which involve fast cooling rates associated with tensile stresses, and particularly during laser welding. Thus, one important point is to reproduce the same fracture mode as encountered in hot tearing of laser welds of the same materials, and to check that the solidification microstructure is qualitatively the same as that in the nugget of such welds (a detailed study of the weld microstructure can be found elsewhere [22]). Fig. 6 shows the microstructure close to the fracture surface of a tensile sample with a 2% Si concentration, and the associated fracture surface, in comparison with similar micrographs for a weld of identical nugget composition. The conditions of the non-isothermal tensile test were chosen so that fracture occurred in the mushy state.

Both solidification microstructures are equiaxed. The grain size is, however, different (500 μm in our experiments, 100 μm in the weld). The secondary dendrite arm spacing is in a similar range in the two cases: 5 μm in the laser weld and about 9 μm in the non-isothermal tensile test. This difference is explained by the difference in cooling rate: 70 K $s^{-1}$ in our experiments (fast cooling rate), compared to approximately 300–400 K $s^{-1}$ in the laser weld. The fracture surfaces look very similar, if one takes into account the scaling effect of the solidification rate. In both cases, one observes only smooth dendrite tips, which are characteristic of fracture along the liquid films in between the solidifying grains, at small liquid fractions.

### 3.2. Tests at slow cooling rate

The mechanical behaviour of the 6056 alloy tested with a cooling rate of 25 K $s^{-1}$ is reported here. Fig. 7 shows the influence of the displacement rate on the stress level. A sharp transition exists between a displacement rate of 0.1 mm $s^{-1}$, where the stress reaches values characteristic of the fully solid state before fracture occurs (50 MPa), and higher displacement rates, where the maximum stress is one to two orders of magnitude smaller in the range 1–2 MPa. Such fracture stresses are characteristic of fracture in the semi-solid state (hot tearing) [23], where cracks propagate along thin liquid films constrained between solidifying grains. This is confirmed by observations of the fracture surfaces associated with the low and high displacement rates (Fig. 8). The material deformed at 0.1 mm $s^{-1}$ exhibits a ductile fracture surface, while the material deformed at 0.4 mm $s^{-1}$ has clearly failed along the liquid films separating neighbouring grains and exhibiting very little solid-state plasticity at the dendrite tips.

For the specimens fractured in the mushy state, the stress increases slowly from the start of loading at a temperature of 613 °C until the temperature reaches 570 °C (solid fraction of 0.95) and then increases sharply until fracture. The maximum stress is observed to increase with increasing displacement rates.

### 3.3. Tests at high cooling rate

For the tensile experiments carried out with cooling at the high rate (70 K $s^{-1}$), the results are presented in terms of stress as a function of fraction of solid, $f_s$. The evolution of the stress is plotted as a function of solid fraction in

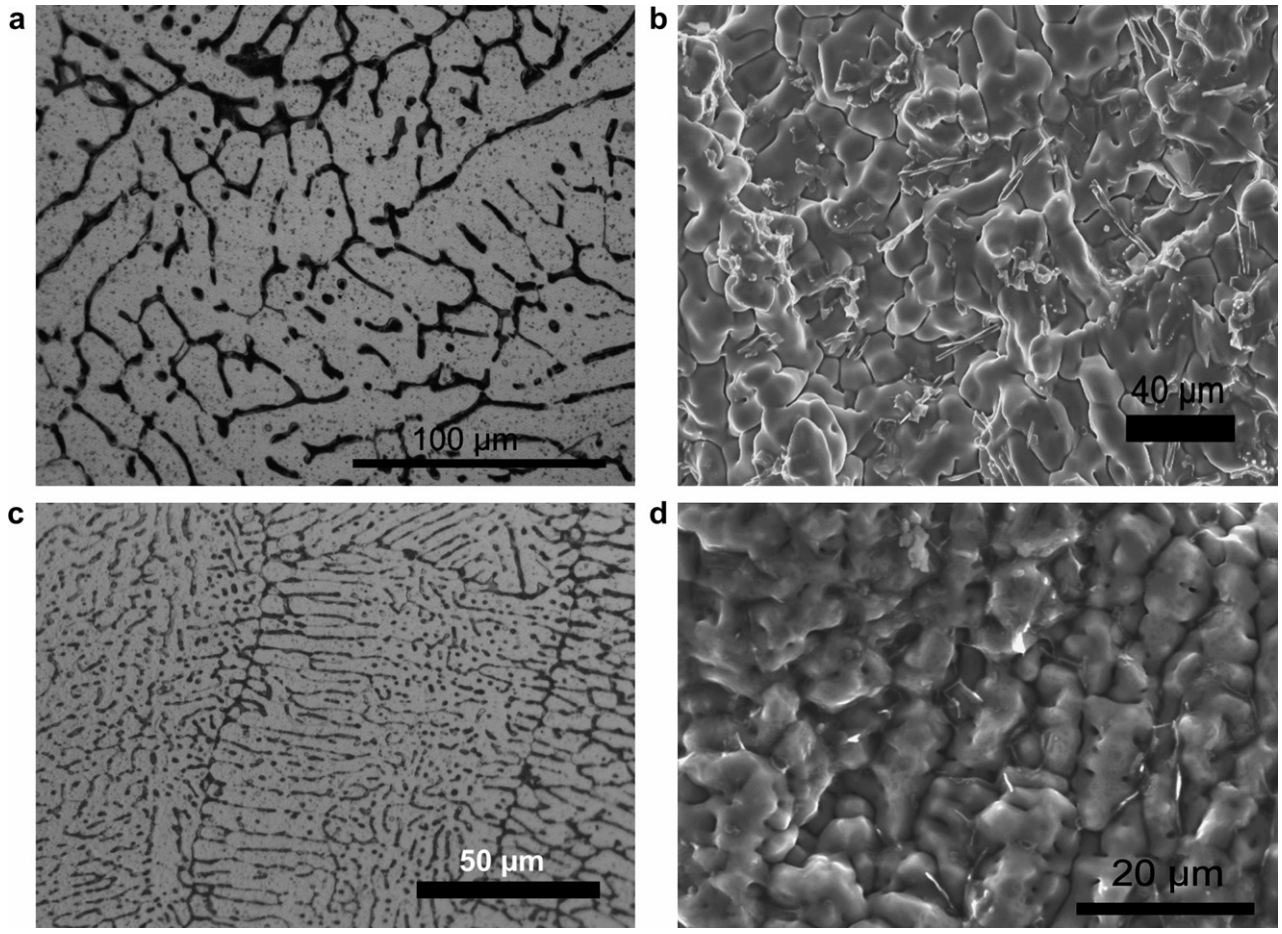


Fig. 6. Comparison between non-isothermal tensile test and laser welding: (a) microstructure of a tensile test using a 2% Si alloy; (b) fracture surface of a tensile test carried out at a displacement rate of 1.5 mm $s^{-1}$ on a 2% Si alloy; (c) microstructure of the fusion zone in a laser weld; (d) fracture surface of a hot tear in a laser weld.

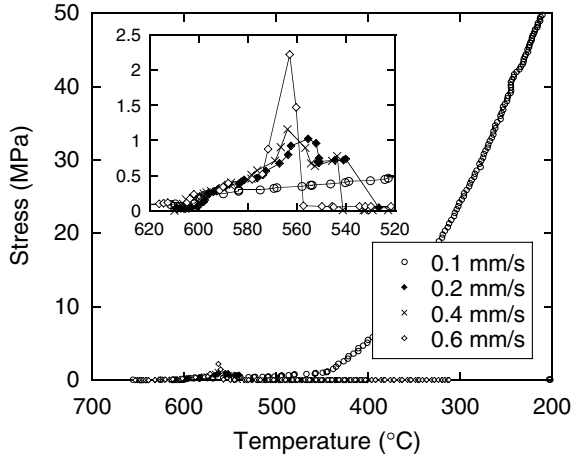


Fig. 7. Measured stress as a function of temperature during a non-isothermal tensile test at slow cooling rate (25 K $s^{-1}$) for different displacement speeds.

Fig. 9 for different imposed displacement rates. A similar behaviour is observed as compared to the slow cooling rate, although it is slightly more complex:

- At high displacement rates (around 2 mm $s^{-1}$), the stress increases sharply when deformation is applied, leading to instantaneous failure. It can be assumed that this behaviour represents essentially the loading of the remaining liquid films between the solidifying grains.
- At intermediate displacement rates, the stress increase is more gradual. A stress plateau at about 1 MPa is observed for the slowest displacement rates (around 1 mm $s^{-1}$). When fracture has not occurred before the solid fraction of 0.95, the stress increases sharply at this solid fraction, similarly to the slow cooling experiments. The transition to fracture in the solid state occurs at about 1 mm $s^{-1}$. This transition rate is unsurprisingly considerably larger than in the case of the slow cooling rate.

### 3.4. Influence of alloy composition

Different alloy compositions, namely the 6056 base alloy and alloys prepared by mixing this alloy with the Al–Si eutectic alloy (AA4047) were tested. Two Si contents, 2 and 4 wt.% Si, were obtained. The addition of Si obviously

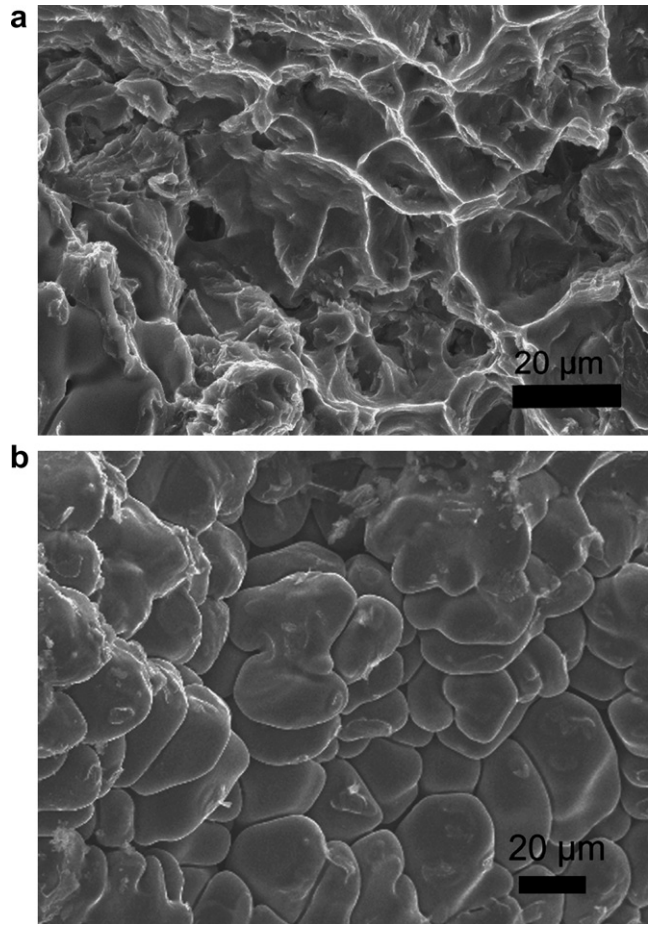


Fig. 8. Fracture surface obtained after non-isothermal tensile test at a slow cooling rate with 6056 alloy: (a) at a displacement speed of 0.1 mm $s^{-1}$; (b) at a displacement speed of 0.4 mm $s^{-1}$.

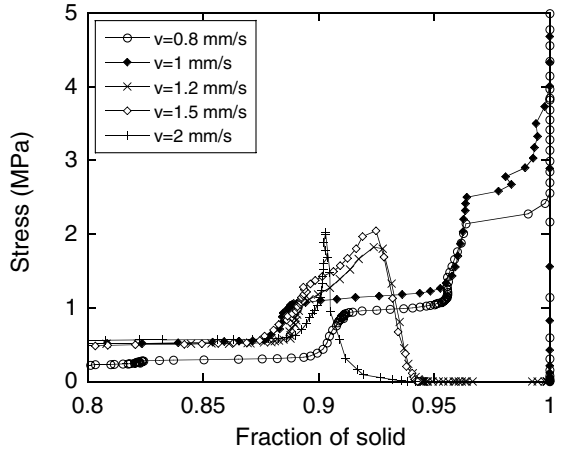


Fig. 9. Measured stress as a function of the solid fraction during non-isothermal tensile test at high cooling rate (70 K $s^{-1}$) for different displacement rates.

changes the solidification path, not only in terms of the temperature range of the solidification interval, but also in terms of the shape of the solid fraction vs. temperature curve. This is illustrated in Fig. 10, where the solidification paths computed by Prophase are plotted for the three alloys. It is shown that in rapid solidification conditions, the 2% and 4% Si alloys show a much larger amount of eutectic phase compared to the 6056 alloy; therefore it can be expected that the mechanical behaviour in the mushy state at high fractions of solid will be markedly different.

Fig. 11 shows the evolution of the stress as a function of the solid fraction during the non-isothermal straining of the three materials, at 1.5 mm $s^{-1}$. For all materials the crosshead displacement is started at a solid fraction of 0.84 (corresponding obviously to different temperatures); however, both the maximum stress and the solid fraction at fracture are considerably reduced when the Si content is increased. Comparison between solid fraction at fracture and solid fraction at the onset of eutectic formation reveals that fracture occurs as soon as the eutectic mixture has formed in all three alloys. One point is to know whether the displacement rate at the transition between fracture in

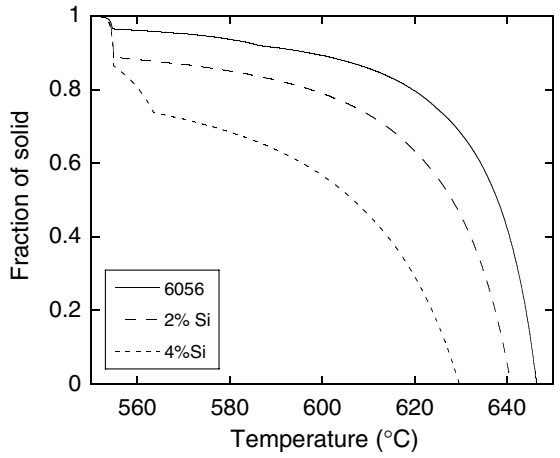


Fig. 10. Solid fraction as a function of temperature (calculated by Prophase software) for the 6056 and the 2% and 4% Si alloys.

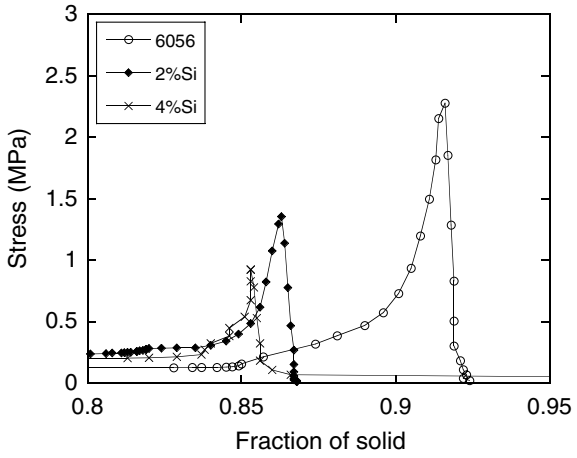


Fig. 11. Measured stress as a function of the solid fraction during a non-isothermal tensile test at high cooling rate (70 K $s^{-1}$) for the different alloys.

the semi-solid state (hot tearing) and fracture in the solid state is the same for the different alloys. Fig. 12, which represents the maximum stress as a function of displacement rate, shows that this critical displacement rate does depend on the alloy composition: for a displacement rate of 0.4 mm $s^{-1}$, the 4% Si alloy fractures at less than 2 MPa (thus in the mushy state), whereas the 2% Si alloy fractures at 16 MPa (thus in the solid state). At 0.3 mm $s^{-1}$, however, the 4% Si alloy fractures at 17 MPa, a level characteristic of the solid state.

The difference in fracture mode at a displacement rate of 0.4 mm $s^{-1}$ is further demonstrated by the fracture surfaces, shown in Fig. 13. The 2% Si alloy shows a mostly ductile fracture surface, whereas the 4% Si alloy exhibits a smooth dendritic surface.

### 3.5. Influence of a grain refiner

It has been observed during the high cooling rate experiments, that the relationship between stress and solid fraction exhibits different shapes, depending on the displacement rate. In some cases, a stress plateau is observed, while for higher cooling rates the stress increase with increasing solid fraction is more abrupt. In order to determine if these different behaviours may be related to the grain structure, experiments with grain-refined alloys were carried out. Fig. 14 shows the variation of stress with solid fraction for the refined and the un-refined AA6056, at three displacement rates.

At the fastest displacement rate (2 mm $s^{-1}$), both materials show a similar, abrupt increase of stress at a solid fraction of about 0.85 until fracture. The refined alloy shows a slight stress plateau, which is, however, not very significant at this stage.

At the lowest displacement rate (0.8 mm $s^{-1}$), both materials show exactly the same behaviour: an initial stress increase at a solid fraction of 0.84, followed by a stress plateau at about 1 MPa, and an abrupt increase of stress at $f_s = 0.95$ until final fracture.

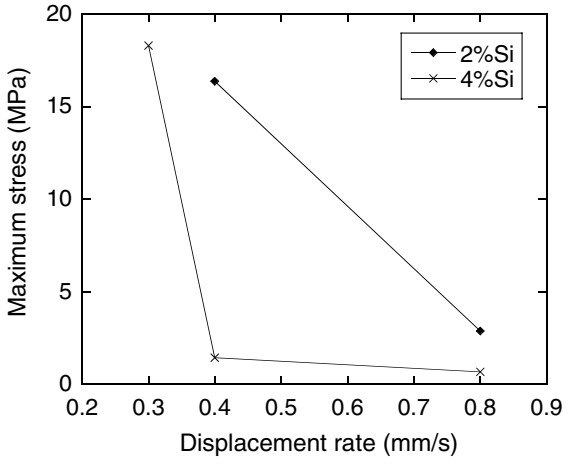


Fig. 12. Maximum measured stress as a function of displacement rate during a non-isothermal tensile test at high cooling rate (70 K $s^{-1}$) for the 2% and 4% Si alloys.

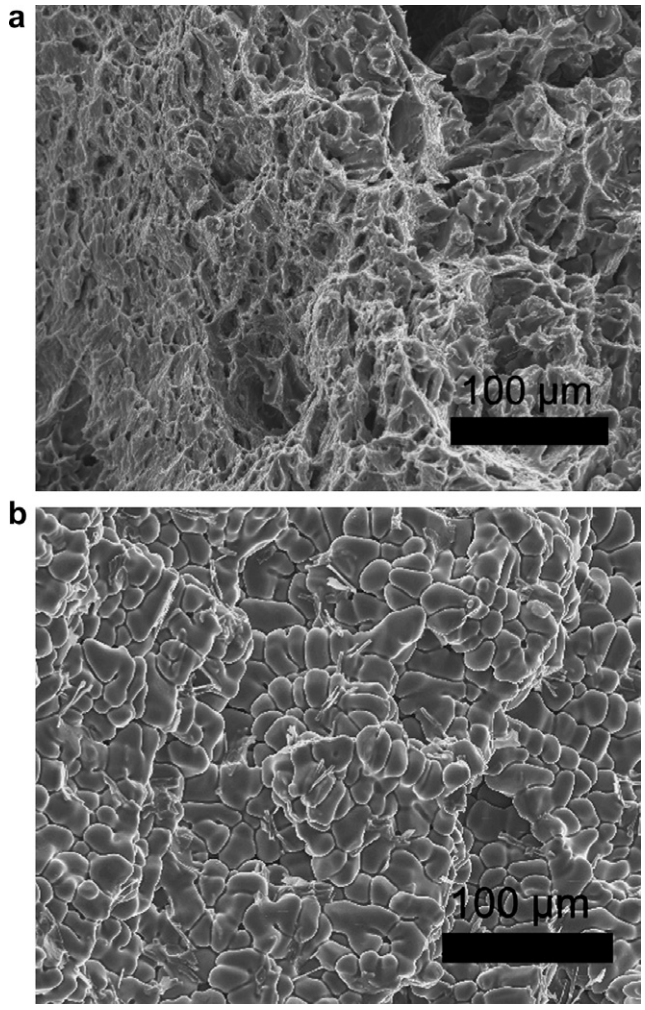


Fig. 13. Fracture surface obtained after non-isothermal tensile test at a high cooling rate at a displacement speed of 0.4 mm $s^{-1}$ (a) for the 2% Si alloy and (b) for the 4% Si alloy.

At an intermediate displacement rate, however, the two materials behave completely differently. The unrefined material exhibits a stress curve characteristic of the fast displacement rate, whereas the curve for the refined material is characteristic of the slow displacement rate. This result shows that there is a well-defined transition displacement rate between the behaviours at slow and at fast strain rates; this value depends on the grain structure.

### 3.6. Displacement before fracture

The ability of a partially solidified material to resist hot tearing is not only related to the maximum stress that it can sustain, but also to its ability to deform before fracture when subjected to an imposed strain. This property has been evaluated during the non-isothermal tensile tests, as the real displacement imposed on the specimen until the maximum stress is reached which corresponds to fracture. Fig. 15 shows the displacement at fracture as a function

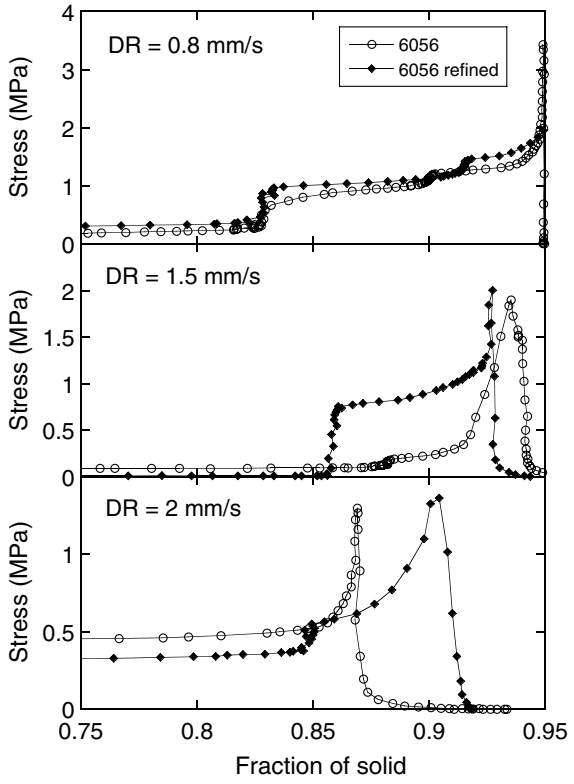


Fig. 14. Measured stress as a function of solid fraction during a non-isothermal tensile test at high cooling rate (70 K $s^{-1}$) for three displacement rates (DR) for the unrefined and the grain-refined 6056 alloy.

of the displacement rate for the three investigated materials (6056, 2% and 4% Si). For a given alloy composition, the displacement at fracture is very different when the fracture occurs in the solid state (large displacement at fracture) or in the semi-solid state (low value). A sharp transition between the two fracture mechanisms is observed, similarly to the transition in maximum stress. An interesting feature is that the displacement at fracture is observed to be constant as a function of displacement rate, in the range where fracture occurs in the mushy state. This constant value, however, is observed to depend on alloy composition: the lower the Si content, the higher the displacement to fracture. It also depends on the cooling rate, as shown in Fig. 16: the lower the cooling rate, the higher the displacement to fracture.

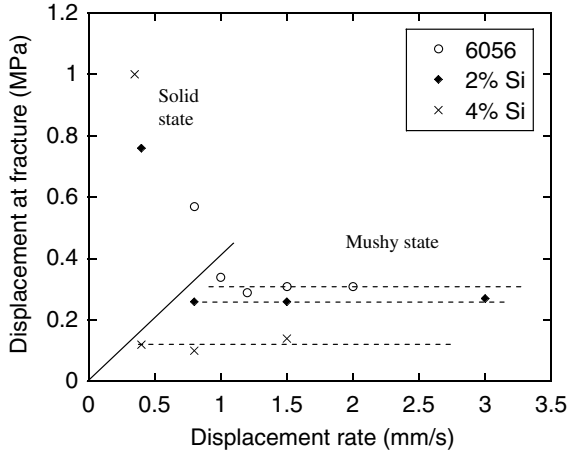


Fig. 15. Displacement at fracture as a function of the displacement rate for non-isothermal tensile test at high cooling rate (70 K $s^{-1}$) for the different compositions.

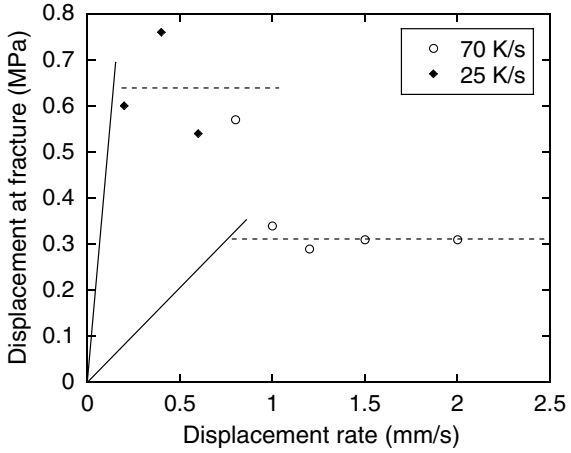


Fig. 16. Displacement at fracture as a function of the displacement rate obtained with the 6056 alloy for two cooling rates.

## 4. Discussion

### 4.1. Mechanical properties of the mushy state before fracture

One of the important results reported above is that the mechanical behaviour in the mushy state can be classified in two characteristic categories when a constant displacement rate is applied during solidification. For high displacement rates, the curves exhibit only a fast stress increase and fracture occurs rapidly. For slow displacement rate, the curves exhibit a more complex shape. When the tensile strain rate is applied, there is an initial increase of the stress to a value of 0.5–1 MPa. Then a stress plateau is observed. Finally, when the solid fraction reaches 0.95, the stress increases sharply. This last stage can be explained by the transition between a mushy state, where almost all the solidifying grains are separated by liquid films so that the mechanical properties are mostly controlled by the liquid phase (before $f_s = 0.95$), to a state where the solid skeleton is significantly connected. The solid fraction of 0.95 at which this transition occurs corresponds to the so-called fraction of coalescence found in the literature [24,25].

The presence of a stress plateau (which corresponds to a significant displacement at constant stress) before the formation of a fully coherent solid skeleton suggests that a rearrangement of the solidifying grains happens, by movement of liquid towards the zones under maximum tension [26]. This interpretation is consistent with the influence of grain refinement: indeed, the behaviour of the grain-refined material is identical in the cases of a very slow or a very fast

displacement rate, but the critical displacement rate differs markedly from the unrefined material. It can actually be expected that the deformation mechanisms are identical in both materials, but that the grain rearrangement can occur much more rapidly in the refined material owing to a much smaller grain size, resulting in a stress plateau at higher displacement rates.

Considering the influence of the Si content, we have observed that fracture occurs at lower stress when the Si content is higher, and that the associated displacement before fracture is lower, which means that fracture is more brittle. We have seen also that fracture occurs as soon as the eutectic phase forms for the 2% Si and the 4% Si alloys. We propose two explanations for this "embrittlement" by the addition of Si. Firstly, in the case of the high-Si alloys (2% and 4%), when the solid fraction is such that interdendritic bridges should form, an extra energy may be necessary to create an interphase between the α phase dendrite (aluminium-rich matrix) and the eutectic bridge. This could result in a lower area fraction of intergranular bridges for a given fraction of solid as compared to the 6056 alloy, where α–α bridges can form due to the low fraction of eutectic phase. This can explain the lower value of the maximum stress. Secondly, the eutectic phases, which are formed between the grains in the high-Si alloys, are rather brittle. When the partially solidified material is strained, there is a competition between plastic deformation of the interdendritic bridges and crack propagation at the grain boundaries. It is consistent that when the Si content is higher, the fracture strain is lower, since the volume fraction of brittle phase constituting the interdendritic bridges is larger.

### 4.2. Fracture mode and displacement to fracture

Our experimental results have shown that a critical displacement rate (CDR) can be defined at the transition between fracture in the mushy state (occurring by separation of grains along the remaining liquid films) and fracture in the solid state (with a clear ductile character). If the displacement rate is lower than the CDR, fracture occurs in the solid state for high stresses and high displacements. This CDR depends on the cooling rate: for a given alloy composition, the CDR increases with increasing cooling rate. It is also observed that in the hot tearing regime (i.e. when the displacement rate is higher than the CDR) this displacement to fracture does not depend on the displacement rate. Figs. 15 and 16 demonstrate, however, that it depends markedly on the alloy composition: the CDR decreases with increasing Si content.

Based on these results, a map describing the conditions of fracture in the mushy state can be drawn as a function of the different parameters investigated, which can be translated in a criterion for fracture by "hot tearing", i.e. fracture along the liquid films. This new criterion for fracture of liquid films consists of two conditions that need to be met simultaneously:

(i) the displacement rate must be higher than the critical one which is a function of the solidification rate and of the Si content;
(ii) fracture occurs if the total displacement applied to the mush is higher than the critical displacement which is also function of the same two parameters.

It should to be pointed out that both the critical displacement rate and the critical strain to fracture depend strongly on the cooling rate. The critical displacement rate can be expected to scale linearly with the cooling rate, if the solidification conditions are not changed (e.g. solidification interval). The situation is less simple for the critical strain to fracture. This depends on the cooling rate, which probably comes from the increased ability for the grains to rearrange when the cooling rate is lower. However, the nature of this dependence is not straightforward to predict. In a first approximation it can be assumed that it scales with the inverse of the cooling rate.

This criterion could be integrated in the modelling of any process for which solidification of aluminium alloys takes place with high solidification rate. If the displacement rate and the total displacement are predicted at any location, this criterion can indicate if there is any risk for hot tearing. However, the plasticity of the mushy state is not negligible, and such a criterion should be coupled with a rheological model capable of predicting the deformation response of a material as a function of the applied stress, temperature, fraction of solid, etc.

### 4.3. Modelling the mechanical response during the non-isothermal tensile test

In a previous paper [3], a constitutive law for the mushy state has been presented. This law is suited to materials partially solidified with high cooling rate before being tensile tested. This law, the parameters of which have been identified in isothermal tensile experiments, describes the strain rate of the partially solidified material as a function of the applied stress, as first suggested by Van Haaften et al. [27]:

$$\dot{\varepsilon} = A\left(\frac{\sigma}{1 - f_{\mathrm{GBWL}}}\right)^{n} \exp\left(-\frac{Q}{RT}\right) \tag{1}$$

where $f_{\mathrm{GBWL}}$ is the fraction of grain boundaries wetted by the liquid, and $A$, $Q$, and $n$ are material parameters. The relationship between the fraction of liquid and the fraction of grain boundaries wetted by the liquid has been calibrated in order to match the mechanical behaviour during the isothermal tensile tests [3]. The material parameters have been extracted from compression tests carried out at high temperature below the solidus. Table 2 gathered the values of the parameters found for the 6056 and the 2% Si alloy. This law describes accurately the maximum stress obtained during isothermal tensile tests for different temperatures and strain rates [3].

Table 2
Values of material parameters derived from compression tests at high temperature

| | $A$ (MPa$^n$ s)$^{-1}$ | $Q$ (kJ mol$^{-1}$) | $n$ |
|---|---|---|---|
| 6056 | 30 | 360 | 15.4 |
| 2% Si | 35 | 305 | 12.9 |

This constitutive law is now used to model the mechanical behaviour during the non-isothermal tensile tests. The first step of the model is to predict the temperature field during the tensile test. Thermocouples were placed in the sample during selected tests and a numerical simulation was carried out using the Calcosoft® software [28]. This thermal field is then translated into a field of solid fractions using the Prophase curves presented in Fig. 10. The distribution of the fraction of solid in the sample is presented in Fig. 17 at different times (time = 0 corresponding of the beginning of the test). The solid fraction is then associated with a fraction of grain boundaries wetted by the liquid, using the relationship developed in a previous paper [3], and thus to a strain rate for a given macroscopic stress. The average strain rate of the specimen is then calculated by integrating the local strain rates corresponding to the local solid fractions along the specimen. This calculated strain rate must be equal to the applied strain rate which gives the value of the calculated stress. This procedure is repeated for each time step to give finally the stress response of the specimen during the non-isothermal tensile test. The numerical integration is carried out using the Scilab® software.

Fig. 18 shows the predicted evolution of the stress when the solidifying sample is subjected to a non-isothermal tensile test for different displacement speeds and two compositions. The simulation predicts that the stress increases to about 1 MPa when the tensile deformation is applied and then increases slowly until a solid fraction of about 0.96 is reached. From that point, the stress begins to increase sharply. This corresponds well to the experimental situations. This very simple model is therefore capable of

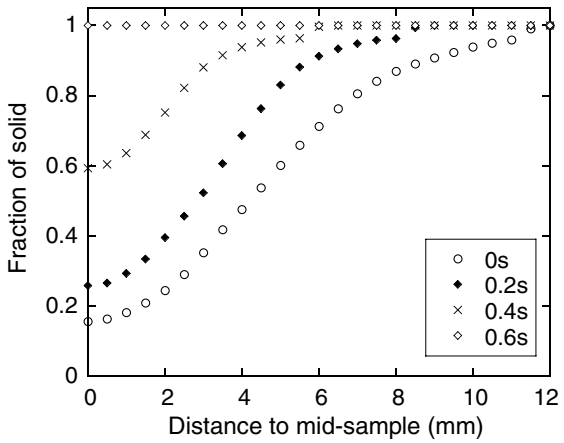


Fig. 17. Solid fraction as a function of the distance to mid-sample during a non-isothermal tensile test at high cooling rate (70 K s$^{-1}$) calculated by Calcosoft® software ($t = 0$ corresponds to the beginning of the test).

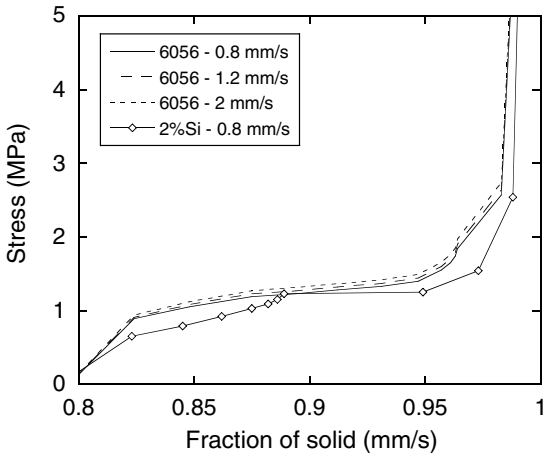


Fig. 18. Simulated stress as a function of solid fraction during non-isothermal tensile test at high cooling rate (70 K s$^{-1}$) for the 6056 and the 2% Si alloy for different displacement rates.

describing, at least in a qualitative way, the complex phenomena occurring during the non-isothermal tensile test.

However, the limits of this model must be discussed. Firstly, the model does not integrate the complex effect of the displacement speed as observed in Fig. 9. Owing to the simplicity of Eq. (1), the model cannot reproduce the transition observed as a function of the displacement rate. This model is suitable for studying the mechanical response of the mush in the case where intermediate displacement rates are imposed. This is representative of the hot tearing phenomenon characterised by fracture occurring at high solid fractions. Another limit of this model has to do with the influence of the alloy composition. The composition of the alloy is taken into account through the material parameters $A$, $Q$, and $n$. This leads to a poor sensitivity of the model to the Si content. A possible improvement of the model would be to consider, according to the composition of the alloy, a different relationship giving the fraction $f_{GBWL}$ as a function of the liquid fraction. Indeed, for the same solid fraction, the liquid phase may be spatially distributed in various ways depending on its composition as solid–liquid interface energies might depend on solute contents. Similarly the influence of the presence of the grain refiner is not taken into account in Eq. (1). Nevertheless, modification of the relationship between $f_{GBWL}$ and liquid fraction is possible to account for the effect of grain size on the distribution of the liquid phase in the mush.

### 4.4. Application to welding

It is worth considering now the final goal of our study, i.e. the hot tearing phenomenon during laser welding of aluminium alloys. It is usually admitted that the use of Al–Si alloy as a filler wire decreases the hot tearing susceptibility of a weld. Numerous studies have confirmed that, as the Si content increases, the hot tearing susceptibility increases until the maximum solubility of Si in Al is reached, and then decreases rapidly [29–31]. Our results

show that the influence of the Si content on the hot tearing susceptibility is not that straightforward. Actually, increasing the Si content results in a decrease of the intrinsic mechanical properties (stress and strain to fracture) when the partially solidified material is subjected to strain. The benefit of the addition of a Si-rich filler wire on hot tearing susceptibility could have several explanations. One could be that the Si content changes the microstructure of the mush and particularly the spatial distribution of the grains. This could lead to the possibility of the grains rotating and moving as in the case of the grain-refined alloy, resulting finally in delayed fracture. Another possibility is that Si changes the wetting angle between the liquid and the solid phase. In a configuration prone to hot tearing, this would permit the liquid to flow more easily and to heal the forming cracks. This cannot be observed during tensile tests since the material that which is strained is that with the lowest fraction of liquid: there is no remaining liquid to heal the forming cracks. Another explanation is that the addition of the filler wire could change the thermal strain applied to the solidifying material: it is known that adding Si to Al reduces the thermal expansion coefficient and the volume change during solidification. If the strain imposed by the solidification process decreases faster than the maximum strain before fracture, the net effect of an increase of the Si content would then be beneficial.

## 5. Conclusions

An original experimental set-up was developed to study the fracture behaviour of Al–Mg–Si–Cu alloys during non-isothermal tensile tests carried out in the mushy state during solidification. The mush exhibits a viscoplastic behaviour and shows a transition between fracture in the solid state and fracture in the semi-solid state when the imposed displacement speed is decreased. This critical speed for the occurrence of rupture in the mushy state depends on the composition of the alloy and on the cooling rate. Decreasing the Si content, increasing the cooling rate, or adding a grain refiner leads to an increase of the critical speed. These experiments also show that the displacement to fracture does not depend on the displacement speed but is a function of the cooling rate and the composition. Based on these two conclusions, a criterion for the occurrence of fracture in the mushy state is suggested which involves a critical strain rate and a critical strain.

The mechanical behaviour of the mush is successfully modelled using a creep-type law in which the fraction of grain boundaries wetted by the liquid is taken into account. As far as the microstructure and the fracture surface observed during these tests are representative of the hot tearing phenomenon, which occurs during laser welding, the model can be used in the simulation of this process. Predictions of the strains involved during solidification would therefore be possible and consequently predictions of the occurrence of hot tearing using a criterion such as that developed in this study. However, differences between fracture in the mushy state during non-isothermal tensile tests and hot tearing during laser welding should be kept in mind. Indeed during laser welding, some remaining liquid can feed the hot tears and heal them, whereas during tensile testing the conditions are much more severe. The addition of a filler wire during welding can also change the physical properties of the mush, and therefore affects the occurrence of hot tearing. Nevertheless, this study is thought to constitute a step towards the understanding of the behaviour of a mush under non-isothermal conditions with a high cooling rate and the conditions of the occurrence of hot tearing during laser welding processes.

## Acknowledgements

The authors are grateful to the French Ministry of Industry for funding in the framework of the ASA (Allègement des Structures dans l'Aéronautique) RNMP project, carried out in collaboration with EADS and ALCAN, which are also thanked for providing the materials.

## References

[1] Dahle AK, Arnberg L. Acta Mater 1997;45:547–59.
[2] Braccini M, Martin CL, Tourabi A, Bréchet Y, Suéry M. Mater Sci Eng A 2002;337:1–11.
[3] Fabrègue D, Deschamps A, Suéry M, Poole WJ. Metall Mater Trans A 2006;37:1459–67.
[4] Sumitono T, StJohn DH, Steinberg T. Mater Sci Eng A 2000;289:18–29.
[5] Nguyen TG, Favier D, Suéry M. Int J Plast 1994;10:663–93.
[6] Gautham BP, Kapur PC. Mater Sci Eng A 2005;393:223–8.
[7] Drezet JM, Rappaz M. Proceedings of TMS light metals. Warrendale, PA: Minerals, Metals and Materials Society; 2001. p. 887–93.
[8] Clyne TW, Davies GJ. Solidif Casting Met 1979:275–6.
[9] Lahaie DJ, Bouchard M. Metall Mater Trans B 2001;32:697–705.
[10] M'hamdi M, Mo A, Martin CL. Metall Mater Trans A 2002;33:2081–93.
[11] Senkara J, Zhang H. Welding Res 2000(July):194–201.
[12] Yang, Yiang JG, Ou BL. Scand J Metall 2001;30:146–57.
[13] Tiang X, Shi Q. J Mater Process Technol 2000;97:30–4.
[14] Guven YF, Hunt JD. Cast Met 1988;1:104–11.
[15] Sigworth GK. AFS Trans 1996:96–155. 1053–62.
[16] Ludwig O. PhD Thesis, INPG, France, 2004.
[17] Campbell J, Clyne TW. Cast Met 1991;3:224–6.
[18] Spittle JA, Brown SGR, James JD, Evans RW. In: Suzaki, Sakai, Matsuda, editors. Proceedings of the 9th symposium on physical simulation of casting, hot rolling and welding, 1996. p. 81–91.
[19] Ackermann P, Kurz W, Heinemann W. Mater Sci Eng A 1985;75:79–86.
[20] Ludwig O, Drezet JM, Martin CL, Suéry M. Metall Mater Trans A 2005;36:1525–35.
[21] Sigli C, Maenner L, Sztur C, Shahani R. In: Sato T, Kumai S, Kobayashi T, Murakami Y, editors. Materials science forum. Proceedings of the 6th international conference on aluminium alloys. Japan Institute of Light Metals; 1998.
[22] Fabregue D, Deschamps A, Suéry M. Mater Sci Technol 2005;21:1329–36.
[23] Dahle AK, Instone S, Sumitono T. Metall Mater Trans A 2003;34:105–13.
[24] Farup I, Mo A. Metall Mater Trans A 2000;31:1461–72.
[25] Rappaz M, Jacot A, Boettinger WJ. Metall Mater Trans A 2003;34:467–79.

[26] Rappaz M. Private communications, Ecole Polytechnique Fédérale de Lausanne, Switzerland, 2004.
[27] Van Haaften WM, Kool WH, Katgerman L. Mater Sci Eng A 2002;336:1–6.
[28] CalcoSoft, user manual, Calcom SA. Available from: http://www.calcom.ch, CH-1015 Lausanne, Switzerland.
[29] Rapp J, Glumann C, Dausinger F, Hugel H. In: Denney P, Miyamoto I, Mordike BL, editors. Proceedings of the 5th international conference on welding and melting by electron and laser beams, 1993. p. 672.
[30] Warrington D, Mc Cartney DG. Cast Met 1989;2:134–43.
[31] Suéry M, Martin CL, Braccini M, Brechet Y. Adv Eng Mater 2001;3:589–93.